

Aging of poled ferroelectric ceramics due to relaxation of random depolarization fields by space-charge accumulation near grain boundaries

Yu. A. Genenko,^{1,*} J. Glaum,¹ O. Hirsch,¹ H. Kungl,² M. J. Hoffmann,² and T. Granzow¹

¹*Institut für Materialwissenschaft, Technische Universität Darmstadt, 64287 Darmstadt, Germany*

²*Institut für Keramik im Maschinenbau, Universität Karlsruhe, 76131 Karlsruhe, Germany*

(Received 31 August 2009; revised manuscript received 26 October 2009; published 22 December 2009)

Migration of charged point defects triggered by the local random depolarization field is shown to plausibly explain aging of poled ferroelectric ceramics providing reasonable time and acceptor concentration dependences of the emerging internal bias field. The theory is based on the evaluation of the energy of the local depolarization field caused by mismatch of the polarizations of neighbor grains. The kinetics of charge migration assumes presence of mobile oxygen vacancies in the material due to the intentional or unintentional acceptor doping. Satisfactory agreement of the theory with experiment on the Fe-doped lead zirconate titanate is demonstrated.

DOI: [10.1103/PhysRevB.80.224109](https://doi.org/10.1103/PhysRevB.80.224109)

PACS number(s): 77.80.Dj, 77.80.Fm, 77.84.Dy, 61.72.jd

I. INTRODUCTION

Many ferroelectric materials exhibit gradual change in parameters with time under equilibrium external conditions, especially when acceptor doped. This phenomenon called aging is known almost as long as ferroelectrics themselves¹ but its mechanism is still highly disputed. Characteristic features of the degradation process are the decreasing dielectric constant and the fixed pattern of the polarization which hinders repolarization of the material. One of the first ideas of the aging mechanism was piling up of the space charge which pins the polarization configuration.²⁻⁶ Until recently, there was, however, no quantitative description of this mechanism which could allow comparison with experiment. An alternative and well-elaborated concept of aging in acceptor-doped ferroelectrics is the mechanism of defect dipole reorientation suggested by Arlt *et al.*^{7,8} and supported in recent works.⁹⁻¹² This concept allowed reasonable explanation of the time and temperature dependencies of the most important parameters of aging, namely, of the emerging internal bias field, E_{ib} , and of the characteristic aging time, τ . Nevertheless, this theory still seems to miss important features of aging concerning its dependence on the doping level. The orientation of the defect dipole due to the random walk of an oxygen vacancy about an acceptor defect is assumed to be a microscopic process independent of the other defect dipoles. Thus, the aging time appears to be independent of the doping level. The internal bias field proportional to the sum of independent contributions of the individual dipoles is expected in this theory to be proportional to the concentration of acceptor defects, c_0 . Experimentally, however, aging time is distinctly c_0 dependent,^{7,13} and the internal bias field saturates with increasing concentration^{13,14} well below $c_0 \approx 1$ mol %. For certain dopants the reason of this saturation could be the solubility limit in the host crystal as is stated to be the case for Fe ions in $\text{PbZr}_x\text{Ti}_{1-x}\text{O}_3$ (PZT) ceramics.^{15,16} The saturation of the bias field is observed, however, for virtually all acceptor dopants below $c_0 \approx 1$ mol % (Refs. 13 and 14) and seems to be a universal feature of acceptor-doped ferroelectrics.

As was recently shown, an alternative, charge-defect migration mechanism can quantitatively explain essential fea-

tures of aging in unpolarized ceramics¹⁷⁻¹⁹ as well as fatigue under a constant electric field.²⁰ Following the latter concepts we advance in this work a model of aging in poled ferroelectric ceramics due to the depolarization-field-driven charge migration. Theoretical results are then compared with model experiments on the PZT ceramics with controlled Fe doping.

II. MODEL OF FULLY POLARIZED FERROELECTRIC CERAMICS

Ferroelectric ceramics are characterized by at least three sorts of randomness: random form of grains, their positions and random orientation of the crystal lattice inside the grains. We assume the last one to be the most important factor of randomness which can capture the main features of aging and fatigue in these systems, therefore only this kind of disorder will be considered in the following.

We imagine the sample to consist of a regular cubic lattice of equal tightly contacted single-crystalline cubic grains of mesoscopic size R much larger than the lattice constant of the material. The grain edges are supposed to be aligned along the axes of the Cartesian coordinate system x, y, z as is shown in Fig. 1.

The sample is supposed to be sandwiched between plane electrodes located at $z = \pm L/2$, where $L \gg R$, and polarized in a dc electric field substantially higher than the coercive field to the maximum possible spontaneous polarization in the z direction. After that the voltage at the electrodes is set back to zero so that the remanent polarization \mathbf{P}_r in the z direction remains. This state is considered as initial one for the process of aging at a fixed temperature and zero voltage maintained.

Since the crystal structure of the grains is formed at temperatures far above the ferroelectric phase transition the crystal axes orientation in different grains is supposed to be absolutely arbitrary and independent. In the high electric field the polarization in every grain takes on the direction of one of the pseudocubic axes most close to the direction of the applied field (see in Fig. 1). Note that the assumption that each grain has a homogeneous polarization is quite strong, as in reality grains always consist of a multitude of domains

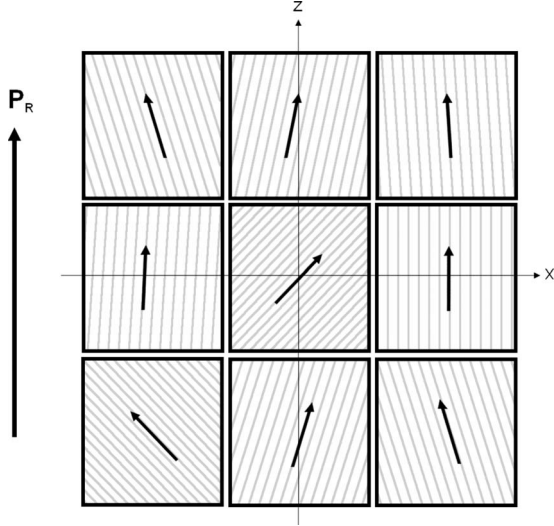


FIG. 1. Two-dimensional projection of polarization distribution in a fully polarized ferroelectric ceramics. Hatching pattern shows schematically the orientation of the crystal lattice.

with different polarization directions. This is a well-known simplification that is often used in literature.^{21,22} Thus, the vectors \mathbf{P}_s of local spontaneous polarization have the same magnitude of P_s and are randomly distributed within the cone defined by the polar angle $\theta < \theta_{\max}$ with respect to the z axis where $\theta_{\max} = \arcsin(\sqrt{2}/3)$ is the threshold angle introduced by Uchida and Ikeda.²² Further simplifying the problem we assume that the achieved maximum polarization in the field direction remains after setting the applied voltage back to zero. For calculation of thermodynamic characteristics one needs a procedure of statistical averaging described in the next section.

A. Configurational averaging

Configurational averaging of local angle-dependent quantities over the ensemble of all possible random configurations, equal to the averaging over the sample volume, may be performed using the distribution function of a possible polarization direction in an arbitrary grain given by

$$f(\theta, \varphi) = \frac{3}{2\pi}, \quad 0 \leq \theta \leq \pi/4 \quad \text{and} \\ = \frac{6}{\pi^2} \left[\frac{\pi}{4} - \arccos(\cot \theta) \right], \quad \pi/4 \leq \theta \leq \theta_{\max} \quad (1)$$

for $0 \leq \varphi < 2\pi$, where φ and θ are the azimuthal and polar angle in spherical coordinates associated with the above-introduced Cartesian coordinates and centered in the center of the chosen grain. The distribution function $f(\theta, \varphi)$ is derived in Appendix A.

Let us introduce a three-dimensional numeration (integer coordinates) of grains $[n, k, m]$ associated with the Cartesian coordinates so that the centers of the grains take positions (nR, kR, mR) . Assuming independence of random angle variables in different grains the distribution function for polarization directions in all grains reads

$$F(\{\theta_i, \varphi_i\}) = \prod_{n,k,m} f(\theta_{n,k,m}, \varphi_{n,k,m}), \quad (2)$$

where $\{\theta_i, \varphi_i\}$ denotes the manifold of spherical angles in all grains, while $\theta_{n,k,m}$ and $\varphi_{n,k,m}$ denote the angles in the grain with numbers $[n, k, m]$.

Calculating an ensemble average of a quantity $g(\{\theta_i, \varphi_i\})$

$$\langle g \rangle = \prod_i \int \sin(\theta_i) d\theta_i \int d\varphi_i g(\{\theta_i, \varphi_i\}) F(\{\theta_i, \varphi_i\}) \quad (3)$$

one should take into account that all azimuthal- and polar-angle variables change in the same ranges as respective angles in Eq. (1). Thus, the ensemble average of the polarization along the z axis, $\langle P_z \rangle$, amounts to

$$P_r = P_s \langle \cos(\theta_{n,k,m}) \rangle = P_s \frac{3\sqrt{2}}{\pi} \arcsin \sqrt{1/3} \quad (4)$$

and equals $0.831P_s$ as in Refs. 21 and 22 while the perpendicular polarization component averages to

$$\langle P_x \rangle = P_s \langle \cos(\theta_{n,k,m}) \cos(\varphi_{n,k,m}) \rangle = 0, \quad (5)$$

as well as $\langle P_y \rangle = 0$. The local polarization can be then conveniently decomposed in a sum of the mean and fluctuation polarizations as $\mathbf{P}_s = \mathbf{P}_r + \Delta\mathbf{P}_s$ where apparently $\langle \Delta\mathbf{P}_s \rangle = 0$.

B. Mean values and variances of charges and fields

Surface bound charge densities at the faces of a cubic grain with the number $[n, k, m]$ located inside the bulk material are constant over the cubic faces and result from discontinuities of the respective normal components of the polarization $\Delta\mathbf{P}_s$ in the neighbor grains. Namely, the charge density at the bottom face perpendicular to the axis z equals

$$\sigma_{n,k,m}^z = P_s [\cos(\theta_{n,k,m-1}) - \cos(\theta_{n,k,m})], \quad (6)$$

the charge density at the left face perpendicular to the axis x equals

$$\sigma_{n,k,m}^x = P_s [\sin(\theta_{n-1,k,m}) \cos(\varphi_{n-1,k,m}) - \sin(\theta_{n,k,m}) \cos(\varphi_{n,k,m})], \quad (7)$$

and the charge density at the left face perpendicular to the axis y equals

$$\sigma_{n,k,m}^y = P_s [\sin(\theta_{n,k-1,m}) \sin(\varphi_{n,k-1,m}) - \sin(\theta_{n,k,m}) \sin(\varphi_{n,k,m})]. \quad (8)$$

Configurational averaging of the above charge densities for internal grains with the function in Eq. (2), equal to the averaging over the sample volume, results in vanishing mean values $\langle \sigma_{n,k,m}^{x,y,z} \rangle = 0$, which does not preclude the fact that local values in Eqs. (6)–(8) are finite. For the top plane of the sample Eq. (6) is not valid because there are no grains above the top grain layer. For that reason the nonzero mean value $\langle \sigma_{n,k,m}^z \rangle = P_r$ produced by the mean polarization \mathbf{P}_r prevails at the top plane of the sample, $z = L/2$. Similarly, $\langle \sigma_{n,k,m}^z \rangle = -P_r$ at the bottom plane of the sample, $z = -L/2$.

Typical magnitudes of the charge densities at the internal grain faces in Eqs. (6)–(8) are characterized by the variances

of the respective charge densities and amount to

$$\begin{aligned}\bar{\sigma}^z &= \sqrt{\langle (\sigma_{n,k,m}^z)^2 \rangle} = 0.142P_s, \\ \bar{\sigma}^{x,y} &= \sqrt{\langle (\sigma_{n,k,m}^{x,y})^2 \rangle} = 0.547P_s.\end{aligned}\quad (9)$$

The substantial difference between $\bar{\sigma}^z$ and $\bar{\sigma}^{x,y}$ is explained by the fact that the direction of the polarization in the (x,y) plane and, hence, variation in its azimuthal angle are not restricted while the polar angle is confined to the cone $\theta \leq \theta_{\max}$ around the positive z direction.

Consistently with the splitting of polarization the total electric depolarization field can be decomposed as $\mathbf{E}_d = \langle \mathbf{E}_d \rangle + \Delta \mathbf{E}_d$ where the mean depolarization field $\langle \mathbf{E}_d \rangle$ is created by the constant charge densities $\pm P_r$ at the planes $z = \pm L/2$, resulting from the mean polarization \mathbf{P}_r , and the fluctuation field $\Delta \mathbf{E}_d$ is created by the fluctuation polarization $\Delta \mathbf{P}_s$. In the considered poled state subject to aging, the field \mathcal{E} created inside the ferroelectric by the external sources (electrodes at $z = \pm L/2$) exactly matches the mean depolarization field so that the mean total electric field $\langle \mathbf{E} \rangle = \mathcal{E} + \langle \mathbf{E}_d \rangle$ vanishes together with the voltage at the electrodes, $V=0$. This means that the mean surface charge densities at the top and bottom planes of the sample are precisely compensated by the opposite charge densities $\sigma = \mp P_r$ at the respective electrodes.

Local depolarization field $\Delta \mathbf{E}_d$ is connected by a nonlocal linear relation with the charge densities at all grain faces. To investigate statistic properties of this field we consider in the following exemplary the field in the center of the central grain with numbers $[0,0,0]$ which is representative for all internal grains of bulk ferroelectric ceramics. This field is given by the tensor relation

$$\Delta E_d^\alpha = \frac{-1}{4\pi\epsilon_0\epsilon_f} \sum_{n,k,m} \sum_{\beta} T_{n,k,m}^{\alpha\beta} \sigma_{n,k,m}^\beta \quad (10)$$

derived in the Appendix B. Here indices α and β are introduced, taking on values x, y, z , and matrix elements $T_{n,k,m}^{\alpha\beta}$ are defined by the integrals over the cubic faces as is shown in the Appendix B. The dielectric tensor of the ferroelectric medium is assumed to be of virtually cubic symmetry and is characterized by the relative permittivity ϵ_f .

Typical magnitudes of the local electric field components are given by respective variances

$$\begin{aligned}\langle (\Delta E_d^\alpha)^2 \rangle &= \left(\frac{P_s}{4\pi\epsilon_0\epsilon_f} \right)^2 \\ &\times \sum_{n,k,m} \sum_{n',k',m'} \sum_{\beta,\beta'} T_{n,k,m}^{\alpha\beta} T_{n',k',m'}^{\alpha\beta'} \langle \sigma_{n,k,m}^\beta \sigma_{n',k',m'}^{\beta'} \rangle,\end{aligned}\quad (11)$$

which are calculated in the Appendix B. The resulting typical field deviations are

$$\sqrt{\langle (\Delta E_d^{x,y})^2 \rangle} = 3.523 \frac{P_s}{4\pi\epsilon_0\epsilon_f},$$

$$\sqrt{\langle (\Delta E_d^z)^2 \rangle} = 0.898 \frac{P_s}{4\pi\epsilon_0\epsilon_f}. \quad (12)$$

The preceding analysis demonstrates that local depolarization fields of the typical magnitude of $P_s/4\pi\epsilon_0\epsilon_f$ are present in the bulk of the grains in the virgin state of poled ferroelectric ceramics. For the PZT materials with $P_s \approx 0.45$ C/m², and the lattice (high-field) value of the permittivity about $\epsilon_f \approx 600$ this field is about 2×10^7 V/m.

C. Evolution of the electric field in the ceramics during aging

If mobile charge carriers are present in the ceramics they have to be driven by the local electric field. Perovskite ferroelectrics are known to be semiconductors with predominantly electronic or hole conductivity in reducing or, respectively, oxidizing atmosphere,^{4,23-29} and a noticeable ionic contribution to the conductivity under the intermediate conditions. Specifically, PZT exhibits domination of ionic conductivity in a wide temperature range at atmospheric oxygen pressure.²⁵ In any case, the density of electronic carriers in the samples quenched from high temperatures to the room temperature is by many orders of the magnitude not sufficient to screen the surface bound charges in the ceramics.^{19,24} In contrast to this, the density of oxygen vacancies, presumably equal to half the concentration of acceptor defects for electroneutrality reasons, is rather large since ferroelectrics are usually unintentionally acceptor doped²⁴⁻²⁶ with small divalent and trivalent cations which substitute for Zr⁴⁺ or Ti⁴⁺. In this work the controlled Fe doping of PZT in the range of 0.1–1 mol % is maintained that results in the oxygen vacancies density of $c_0 \approx 10^{19} - 10^{20}$ cm⁻³, sufficient for screening of spontaneous polarization. An important question concerning the space-charge migration mechanism is: which part of the oxygen vacancies introduced by the acceptor doping is mobile. Measurements of ionic conductivity in Ca-doped barium titanate^{25,26} and in Ni-doped strontium titanate²⁷ show a substantial increase in the conductivity with increasing doping which suggests that a significant part of the introduced vacancies is mobile. On the other hand, the ionic conductivity rises subproportionally with doping which may be the effect of defect association.²⁷ In the following we consider oxygen vacancies, the most mobile ionic species in perovskites, as a suitable agent for slow screening process. A possible effect of the subproportional increase in the mobile vacancy concentration with doping will be considered when adjusting theoretical results to the experimental data.

During the migration of charge carriers they pile up at the charged grain faces to compensate the source of the electric field and thereby produce themselves the electric field \mathbf{E}_M . This process stops when the surface bound charges $\sigma_{n,k,m}^\alpha$ are outweighed by the emerging space charge. The charge redistribution inside the grains may be interpreted as a polarization \mathbf{P}_M , superimposed over the local polarization $\Delta \mathbf{P}_s$. This is indeed a sort of migration polarization systematically studied experimentally by Okazaki in Refs. 2–4. In our model, however, this migration is induced by the fluctuation depolarization field $\Delta \mathbf{E}_d$ which was not considered in the men-

tioned works by Okazaki. Typical thickness of space-charge zones near the faces about $h \approx \bar{\sigma}^\alpha / qc_0$, with the oxygen vacancy charge equal twice the elementary charge q and the vacancy concentration equal to half the acceptor concentration c_0 , amounts to 2–10 nm at $c_0=1$ mol %. This thickness is by two orders of magnitude less than the grain size R . This means that the space-charge density $\sigma_M = h \nabla \mathbf{P}_M$ related to the migration polarization may be simply included in the total time-dependent surface charge $\sigma_{n,k,m}^\alpha(t) = \sigma_{n,k,m}^\alpha(0) + \sigma_M(t)$ where initial values at $t=0$ are given by the virgin charge densities in Eqs. (6)–(8).

The influx of the screening charge to a charged face is driven by the local value of the electric field at the face which consists of the field generated by the face itself and that induced by the other faces. The latter contribution is continuous across the face and does not result in the net change in the surface charge. The former component is normal to the face at its both sides and equals $\sigma_{n,k,m}^\alpha / 2\epsilon_0\epsilon_f$ according to Gauss theorem. Thus the charge changes according to equation

$$\partial_t \sigma_{n,k,m}^\alpha = -\kappa \sigma_{n,k,m}^\alpha / \epsilon_0\epsilon_f, \quad (13)$$

where $\kappa = q\mu c_0$ is the conductivity due to oxygen vacancies with the mobility μ . Consequently, the complicated and random spatial distribution of the depolarization field in the sample remains unchanged during the charge migration while the magnitude of this field scales down coherently at all charged faces of the grains as $\sigma_{n,k,m}^\alpha(0) \exp(-t/\tau_r)$ where $\tau_r = \epsilon_0\epsilon_f / \kappa$ is the Maxwell-Wagner relaxation time. The latter seems to be the only characteristic time for aging mechanism through the charge migration assuming homogeneous background density of acceptor defects.

In fact, there can be reasons for a distribution of this time in a rather wide range. For example, if the activation energy of the mobility is randomly distributed in some range this can result in quasilogarithmic time dependence of material parameters as in the case of aging in unpoled ferroelectrics.^{8,19} Another reason can be the field dependence of mobility as well as the complicated interplay of acceptor charge states and electronic state occupancies because of the band bending by the strong electric field near the charged faces of the grains as was suggested in photochemical studies of PZT.³⁰ The latter phenomena are still beyond the scope of our simple model.

The relaxation time is determined by the concentration and mobility of the oxygen vacancies. The former value is controlled by the acceptor concentration and can be reduced by the possible defect association as was mentioned before. The latter value is still highly disputed. Despite of the wide consensus concerning the migration energy barrier for oxygen vacancies about $E_a = 0.9 - 1.1$ eV (Refs. 25–27 and 31) the reported experimental values of the mobility at temperature $T = 250$ °C range from 8×10^{-9} cm²/V s, obtained by the simultaneous thermoelectric power and conductivity measurements in Refs. 25–27, down to 2×10^{-14} cm²/V s established from the diffusion depth profiles for oxygen tracers at the same temperature in Ref. 31. Estimations at room temperature and the concentration of $c_0 = 1$ mol % result accordingly in a wide range of possible aging times from 10^3 to

4×10^8 s. In the Ref. 31, however, the strongly donor doped (1–4 mol % of Nb⁵⁺) PZT ceramics were studied in contrast to the acceptor-doped ceramics of the Refs. 25–27 which could have effect on the oxygen-tracer mobility. In the following we will rely on the ionic conductivity measurements of the acceptor-doped PZT ceramics.²⁵

D. Thermodynamic analysis

Considering the Gibbs free energy for ferroelectrics, Eq. (C2) of Appendix C, for the sample in the uniform external field exactly compensating the mean depolarization field, $\mathcal{E} = -\langle \mathbf{E}_d \rangle$, the contribution of the conductors $\sim \sigma V$ vanishes because of the zero voltage at the electrodes, $V = 0$, resulting in the initial energy before aging starts

$$G = F_0 \Omega - \frac{1}{2} \int dV \Delta \mathbf{P}_s \Delta \mathbf{E}_d, \quad (14)$$

where Ω is the sample volume. The latter term here presents the contribution of the local fluctuations of the field and the polarization to the total energy of the system and equals at $t=0$

$$\Delta G_+(0) = -\frac{1}{2} \Omega \sum_\alpha \langle \Delta P_s^\alpha \Delta E_d^\alpha \rangle = 0.649 \frac{P_s^2 \Omega}{4\pi\epsilon_0\epsilon_f} \quad (15)$$

as is evaluated in the Appendix B. In the course of aging the local field and polarization are modified as $\Delta \mathbf{P}_s \rightarrow \Delta \mathbf{P}_s + \mathbf{P}_M(t)$ and $\Delta \mathbf{E}_d \rightarrow \Delta \mathbf{E}_d + \mathbf{E}_M(t)$ and decrease as $\sim \exp(-t/\tau_r)$. Thereby the fluctuation contribution to the energy becomes

$$\Delta G_+(t) = -\frac{1}{2} \int dV [\Delta \mathbf{P}_s + \mathbf{P}_M(t)] [\Delta \mathbf{E}_d + \mathbf{E}_M(t)]. \quad (16)$$

This energy decreases with time $\sim \exp(-2t/\tau_r)$ from the initial positive value, Eq. (15), driving the system to an energy minimum which means pinning of the given macroscopic polarization state. The strength of this pinning is characterized by the internal bias field which can be evaluated as follows.

When reversing the external field to the opposite direction after the aging time t the local polarization and field change as $\mathbf{P}_s \rightarrow -\mathbf{P}_s$ and $\mathbf{E}_d \rightarrow -\mathbf{E}_d$. Thereby the fluctuation contribution to the energy changes to

$$\Delta G_-(t) = -\frac{1}{2} \int dV [-\Delta \mathbf{P}_s + \mathbf{P}_M(t)] [-\Delta \mathbf{E}_d + \mathbf{E}_M(t)], \quad (17)$$

where $\mathbf{P}_M(t)$ and $\mathbf{E}_M(t)$ remain unchanged because the charge defects are too slow to follow the repolarization immediately. Taking into account that $\mathbf{P}_M(t) = -\Delta \mathbf{P}_s [1 - \exp(-t/\tau_r)]$ and $\mathbf{E}_M(t) = -\Delta \mathbf{E}_d [1 - \exp(-t/\tau_r)]$ the difference in the energy of the opposite poled states amounts to

$$\begin{aligned}\Delta G_{-}(t) - \Delta G_{+}(t) &= \int dV[\Delta\mathbf{P}_s\mathbf{E}_M(t) + \mathbf{P}_M(t)\Delta\mathbf{E}_d] \\ &= 4\Delta G_{+}(0)[1 - \exp(-t/\tau_r)].\end{aligned}\quad (18)$$

Considering the increase in energy, which should be overcome by the repolarization, one can introduce an effective internal bias field as it was done by Arlt and Neumann⁷

$$\begin{aligned}E_{ib}^{\parallel}(t) &= \frac{[\Delta G_{-}(t) - \Delta G_{+}(t)]}{P_s\Omega} \\ &= A\frac{P_s}{4\pi\epsilon_0\epsilon_f}[1 - \exp(-t/\tau_r)],\end{aligned}\quad (19)$$

where $A=2.597$ was calculated using Eq. (15). The maximum value of this field achieved at times $t \gg \tau_r$ is about 1.7×10^7 V/m which is in agreement with experimental estimations in Ref. 4 but exceeds by one order of the magnitude the values reported in Refs. 13 and 14. Very high theoretical values of the saturated bias field may follow from the basic hypothesis of the model on the absence of any correlations between polarizations in neighbor grains. That assumption allows appearance of unfavorable local configurations with high charge at the grain faces which can in reality be substantially depressed by local correlations. This fact will be considered below by adjusting the experimental curves.

When applying to the aged sample the external field in the perpendicular direction as it is done in some experiments¹⁰ the fluctuation contribution becomes

$$\Delta G_{\perp}(t) = -\frac{1}{2} \int dV[\Delta\mathbf{P}_s^{\perp} + \mathbf{P}_M(t)][\Delta\mathbf{E}_d^{\perp} + \mathbf{E}_M(t)].\quad (20)$$

The fluctuation polarization in this state, $\Delta\mathbf{P}_s^{\perp}$, is correlated neither with the initial fluctuation polarization $\Delta\mathbf{P}_s$ nor with the field $\Delta\mathbf{E}_d$, therefore $\langle\Delta\mathbf{P}_s^{\perp}\mathbf{E}_M(t)\rangle=0$ and, for the same reason, $\langle\mathbf{P}_M(t)\Delta\mathbf{E}_d^{\perp}\rangle=0$. On the other hand, $\langle\Delta\mathbf{P}_s^{\perp}\Delta\mathbf{E}_d^{\perp}\rangle = \langle\Delta\mathbf{P}_s\Delta\mathbf{E}_d\rangle$ since the system is macroscopically isotropic and this mean value should be direction independent. Consequently, the excess energy by the repolarization in perpendicular direction amounts to

$$\begin{aligned}\Delta G_{\perp}(t) - \Delta G_{+}(t) &= \frac{1}{2} \int dV[\Delta\mathbf{P}_s\mathbf{E}_M(t) + \mathbf{P}_M(t)\Delta\mathbf{E}_d] \\ &= 2\Delta G_{+}(0)[1 - \exp(-t/\tau_r)],\end{aligned}\quad (21)$$

and the internal bias field in the perpendicular direction is then equal half that in the initial polarization direction, $E_{ib}^{\perp}(t) = (1/2)E_{ib}^{\parallel}(t)$.

We stress that the maximum magnitude of the bias field, Eq. (19), achieved at times $t \gg \tau_r$, is defined by the energy of the fluctuation electrostatic field, $\Delta G_{+}(0)$. This energy, Eq. (15), is proportional to the volume of the sample and, thus, is at least one order of the magnitude higher than the corresponding energy in the case of the unpoled ferroelectrics,¹⁹ which is accumulated near the charged domain faces. If the defect concentration in the bulk is so large that $c_0 \gg c^* = \bar{\sigma}^{\alpha}/qR$ and, hence, the thickness of the space-charge zone $h \ll R$, the whole energy of the fluctuation electrostatic field

is virtually suppressed in the course of aging and, therefore, the maximum value of E_{ib} becomes concentration independent. In fact, the grain size R itself is doping dependent in the considered material which is typical for ferroelectric ceramics⁴ so that it is about $10 \mu\text{m}$ at $c_0=0.1$ mol % and decreases to $1 \mu\text{m}$ at $c_0=1$ mol %. Thus, $h \ll R$ seems to be always the case. An apparent c_0 dependence of the measured E_{ib} may arise, however, due to the concentration dependence of the relaxation time τ_r . Thus, at the initial stage of aging, $t \ll \tau_r$, the bias field equals $E_{ib}(t) \sim t/\tau_r \sim c_0$.

III. EXPERIMENT ON PZT

To study the effect of doping on aging, PZT bulk samples with a zirconia to titania ratio of 54/46 were prepared with controlled contents of iron by a mixed oxide route.³² Undoped samples were used as well as samples doped with 0.1, 0.5, and 1 mol % of Fe. The powders were calcined, pressed into cylindrical bodies and sintered at 1050 °C in air for 6 h. The bodies were cut into disk-shaped samples with a wire saw (Well 2420, Well Diamantdrahtsaegen GmbH, Mannheim, Germany) and polished down to $3 \mu\text{m}$ grid size. After polishing the samples were relaxed in a furnace at a maximum temperature of 400 °C for 2 h to relieve mechanical stresses that were induced by the cutting and polishing process. Silver electrodes of 50 nm thickness were sputtered on the polished samples and a silver paste (Gwent Electronic Materials Ltd., Pontypool, U.K.) was fired on afterwards at 400 °C.

For the measurements it was necessary to start with fully unaged samples to ensure a statistical distribution of all defects and free charges. If the samples are cooled slowly through the Curie temperature they age very fast and one can only obtain highly pinched hysteresis loops.³³ Therefore the samples were placed short circuited in a furnace at 450 °C for 10 min before the first measurement. This leads to the necessary redistribution of the defects within the sample. After that they were quenched in pure water down to room temperature. By this the statistical charge configuration is “frozen” and the samples can easily be poled and measured in the unaged state.

The polarization measurements were done in a Sawyer-Tower circuit with a 4.78 μF test capacitance. The samples were placed between two soft springs in a silicon oil bath and the bipolar polarization hysteresis loops were measured at a frequency $f=55$ mHz and a maximum field amplitude $E = \pm 2$ kV/mm. The data were recorded by an oscilloscope. For each measurement step two bipolar cycles were applied. The first two cycles lead to the poling of the sample. After poling and measuring the samples were short circuited. Until the next measurement they were kept at room temperature in a sample box. Data points were taken after various time steps between 40 and 10^6 s.

The measured P - E loops were evaluated with respect to the internal bias field E_{ib} , to record the shift of the polarization curve along the field axis depending on the aging time.^{7,13} This field was calculated as follows:

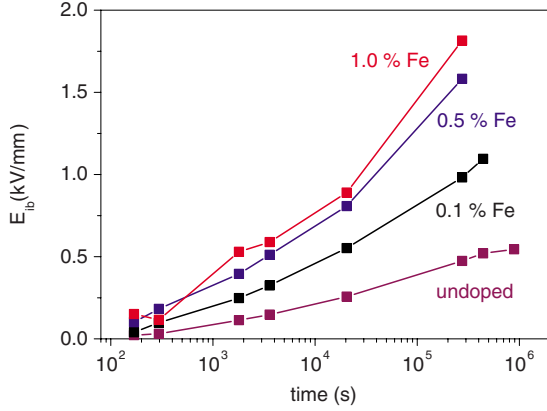


FIG. 2. (Color online) Internal bias field as a function of time for PZT samples with different Fe contents.

$$E_{ib} = -(E_c^- + E_c^+)/2, \quad (22)$$

where E_c^- is the coercive field when a negative external field is applied and E_c^+ is the coercive field on the positive field side.

The internal bias field is presented as a function of time for different Fe contents in Fig. 2. Two common features of these curves are noticeable: they are virtually quasilinear on the logarithmic scale and all of them but one exhibit increasing slope. The first property is characteristic of aging and can be explained assuming wide distribution of relaxation times in the range $\tau_{\min} < \tau_r < \tau_{\max}$,⁸ the second feature means then that the time span of measurements spreads well above τ_{\min} but is still well below τ_{\max} . Wide distribution of times τ_r may follow from a random distribution of activation energies E_a (Refs. 8 and 19) for which there are at least two physical reasons: various positions of the atomic cells with respect to the grain boundary, which can affect E_a , and the mixture of regions with rhombohedral and tetragonal symmetry typical of the systems near the morphotropic phase boundary such as the compound $\text{PbZr}_{0.54}\text{Ti}_{0.46}\text{O}_3$ studied here. We assume in the following that the activation energy is a random variable with a Gaussian distribution $g(E_a) \sim \exp[-(E_a - \bar{E}_a)^2/2s^2]$ of the width $s \approx 0.22$ eV around the mean value $\bar{E}_a \approx 1.12$ eV. The internal bias field is then averaged over this distribution as

$$\bar{E}_{ib}(t) = \int_0^\infty dE_a g(E_a) E_{ib}(E_a, t), \quad (23)$$

where the bias field $E_{ib}(E_a, t)$ is given by Eq. (19) with the relaxation time $\tau_r = \varepsilon_0 \varepsilon_f / q \mu c_0$ defined by the mobility²⁷ $\mu \sim T^{-1} \exp(-E_a/kT)$ with absolute temperature T and the Boltzmann constant k .

By adjustment of the theoretical curves, Eq. (23), to the corresponding experimental ones for different doping concentrations two facts should be taken into account. First, the above-mentioned grain-size dependence on c_0 may have an effect on the maximum value of E_{ib} . Indeed, it is known that larger grains in PZT often contain faults such as subgrains in their crystal structure.³⁴ These faults create regions with different polarization direction, but the correlation between

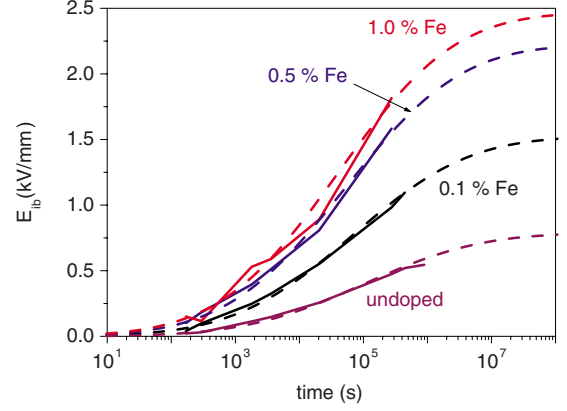


FIG. 3. (Color online) Fitting of the experimental time dependencies of the internal bias field of Fig. 2 (solid lines) with theoretical curves of Eq. (23) (dashed lines) is performed using the following field reduction factors and the effective concentrations of the mobile vacancies (see text): $\alpha=0.141$ and $c_{eff}=0.15$ mol % for $c_0=1.0$ mol %, $\alpha=0.127$ and $c_{eff}=0.12$ mol % for $c_0=0.5$ mol %, $\alpha=0.087$ and $c_{eff}=0.09$ mol % for $c_0=0.1$ mol %, and $\alpha=0.045$ and $c_{eff}=0.06$ mol % for the nominally undoped PZT.

these regions is higher than between neighboring independent small grains. This means higher energy of the fluctuation depolarization fields and, accordingly, higher E_{ib} for smaller grains, i.e., for higher concentration c_0 . Second, accounting for the subproportional increase in the mobile vacancy concentration²⁷ with increasing c_0 and for the presumed solubility limit^{15,16} for Fe in PZT at 0.5–0.8 mol % one should rather use an effective concentration of the mobile vacancies $c_{eff} < c_0$ in the formula (23). For those reasons, the reduction factor for the amplitude of the internal bias field, $\alpha < 1$, and c_{eff} are used as fitting parameters when adjusting experimental results of Fig. 2 with Eq. (23). As is seen in Fig. 3, satisfactory agreement is achieved by $\alpha \approx 0.05-0.1$ and effective concentrations $c_{eff} \approx 0.15$ mol % for $c_0=1.0$ mol %, $c_{eff} \approx 0.12$ mol % for $c_0=0.5$ mol %, $c_{eff} \approx 0.09$ mol % for $c_0=0.1$ mol %, and $c_{eff} \approx 0.06$ mol % for the nominally undoped material. Finally, the presented comparison of the charge migration model with experiments demonstrates that this mechanism may provide the observed magnitudes of the internal bias field and exhibit a reasonable agreement in the characteristic time and doping dependences.

IV. CONCLUSIONS

Even in the state with maximum spontaneous polarization of the ferroelectric ceramics the polarizations of individual grains cannot perfectly match each other all over the material because of random and independent orientation of the crystal lattice in different grains. That is why local bound charges at the grain surfaces and local depolarization field in the bulk are present even if the mean depolarization field is exactly compensated in the electroded sample by zero voltage applied. We tried to capture this important feature of ferroelectric ceramics in the model of perfectly ordered cubic grains

with random crystal-lattice orientation in them. The frozen orientational disorder of the vectors of polarization in the grains can relax to the ordered state if mobile charges are present, which is the case in the acceptor-doped (also unintentionally) ferroelectrics. Driven by the local depolarization field they can partly or completely compensate the fluctuation bound-charge densities at the grain faces by building the thin space-charge zones near these faces. This is equivalent to effective alignment of the local polarizations in the direction of the total polarization accompanied by suppression of the fluctuation depolarization field. The described process leads the system to the energy minimum where it resists its repolarization to another direction, i.e., exhibits aging of the poled ferroelectrics. Quantitative analysis of the relaxation kinetics in our model and its comparison to the model experiments with controlled acceptor contents show reasonable agreement in the magnitude of the internal bias field and its dependence on time and doping. By adjusting the experimental results with theoretical dependencies the activation energy of the vacancies was assumed smeared around the mean value of 1.1 eV, the concentration of the mobile vacancies c_{eff} was taken reduced with respect to the acceptor concentration c_0 and the depression of the internal bias field by the possible correlation between the neighbor grains was taken into account.

The suggested model assumes charge migration in the bulk of the grains which means, in fact, drift over the distance h , the thickness of the space-charge zone. Another screening scenario may occur if the vacancies in the intergranular space are relevant to aging.⁴ The vacancy diffusion along the grain boundaries is known to be two orders of the magnitude faster than the bulk diffusion³¹ but the characteristic distance the charged defects should cover in this mechanism is given by the grain size $R \gg h$. The significance of the grain boundary contribution to screening seems therefore to increase for systems with smaller grains, i.e., by higher acceptor concentrations. This mechanism depends, however, on many still questionable factors, in the first instance, on the concentration of acceptors and oxygen vacancies in grain boundaries^{15,16} and their charge state.³⁰

Though the fluctuation depolarization field is present and causes charge migration in the whole volume of the polarized ceramics the charge defects pile up at the grain boundaries making the considered effect a kind of surface phenomenon. This mechanism does not preclude, however, other possible bulk mechanisms which can contribute to the aging of ferroelectric materials as, for example, the aforementioned defect dipole mechanism. Formation of such Fe-O and Cu-O dipoles in the bulk lead titanate could be detected by means of electron paramagnetic resonance.¹¹ It would be also interesting to prove by spectroscopic methods the presence of deficit or excess free vacancies and, respectively, Fe ions in space-charge zones near the grain boundaries. This would be, however, not easy to detect because the volume share of these zones is about $h/R \sim 10^{-3} - 10^{-2}$.

ACKNOWLEDGMENTS

Useful discussions with Karsten Albe, Rüdiger Eichel,

and Jürgen Rödel are gratefully acknowledged. This work was supported by the Deutsche Forschungsgemeinschaft through the Collaborative Research Center 595.

APPENDIX A: RANDOM DISTRIBUTION OF POLARIZATIONS IN GRAINS

The distribution function $f(\theta, \varphi)$ can be derived following Uchida and Ikeda.²² They considered a domain polarized in the positive z direction and found a random distribution of the electric field, of the magnitude much higher than the coercive field, which is compatible with this direction of the polarization. Due to fourfold symmetry of the problem it is sufficient to consider the azimuthal region $-\pi/4 < \varphi < \pi/4$. A possible 90° rotation of polarization from the z to x axis occurs when the projection of a unit field vector on the z axis, $\cos \theta$, becomes equal to the projection on the x axis, $\cos \theta' = \sin \theta \cos \varphi$. This determines the boundary of the area on the unit sphere $\theta(\varphi) = \arctan(1/\cos \varphi)$. Thus the polar angle at this boundary changes between $\theta = \pi/4$ at $\varphi = 0$ and $\theta_{\max} = \arctan(\sqrt{2})$ at $\varphi = \pi/4$. Within this area, the probability of different field directions which are compatible with the polarization along the z axis is uniformly distributed with distribution function $p(\theta, \varphi) = 3/2\pi$. Averaging of the field projection on the z direction results in $\langle \cos \theta \rangle = 0.831$, in accordance with Eq. (4).

For the aims of this paper, we need a distribution function $f(\theta, \varphi)$ of the possible polarization orientations compatible with the strong electric field applied in the positive z -axis direction. In contrast to the function $p(\theta, \varphi)$ this distribution is obviously not φ dependent since there is no special direction in the x - y plane. We assume here that the crystal lattice orientation is completely decoupled from the form and orientation of grains. The probability for the polarization to occur in the solid angle near the polar angle θ is given by relation

$$2\pi \sin \theta d\theta f(\theta, \varphi) = 8 \int_{\varphi_0}^{\pi/4} d\varphi \sin \theta d\theta p(\theta, \varphi). \quad (\text{A1})$$

So long as the polar angle θ is less than $\pi/4$ the integration over φ in the above integral goes from $\varphi_0 = 0$ to $\pi/4$ which results in the constant value of $f(\theta, \varphi)$. When $\pi/4 < \theta < \theta_{\max}$ the integration goes from $\varphi_0 = \arccos(\cot \theta)$ to $\pi/4$ which results in the function shown in Eq. (1).

APPENDIX B: CALCULATION OF THE LOCAL DEPOLARIZATION FIELD AND ITS MOMENTS

The electric field [Eq. (10)] is calculated by direct summation of contributions from all grain faces charged with densities in Eqs. (6)–(8). Let us introduce notations $n_{\pm} = n \pm 1/2$, $k_{\pm} = k \pm 1/2$, and $m_{\pm} = m \pm 1/2$. Then the matrix elements $T_{n,k,m}^{\alpha\beta}$ in the formula (10) are defined by the integrals over the cubic faces in dimensionless variables $X = x/R$, $Y = y/R$, and $Z = z/R$

$$T_{n,k,m}^{xx} = \int_{k_-}^{k_+} dY \int_{m_-}^{m_+} dZ \frac{n_-}{(n_-^2 + Y^2 + Z^2)^{3/2}}, \quad (\text{B1})$$

$$T_{n,k,m}^{xy} = \int_{n_-}^{n_+} dX \int_{m_-}^{m_+} dZ \frac{X}{(X^2 + k_-^2 + Z^2)^{3/2}}, \quad (\text{B2})$$

$$T_{n,k,m}^{xz} = \int_{n_-}^{n_+} dX \int_{k_-}^{k_+} dY \frac{X}{(X^2 + Y^2 + m_-^2)^{3/2}}, \quad (\text{B3})$$

$$T_{n,k,m}^{yx} = \int_{k_-}^{k_+} dY \int_{m_-}^{m_+} dZ \frac{Y}{(n_-^2 + Y^2 + Z^2)^{3/2}}, \quad (\text{B4})$$

$$T_{n,k,m}^{yy} = \int_{n_-}^{n_+} dX \int_{m_-}^{m_+} dZ \frac{k_-}{(X^2 + k_-^2 + Z^2)^{3/2}}, \quad (\text{B5})$$

$$T_{n,k,m}^{yz} = \int_{n_-}^{n_+} dX \int_{k_-}^{k_+} dY \frac{Y}{(X^2 + Y^2 + m_-^2)^{3/2}}, \quad (\text{B6})$$

$$T_{n,k,m}^{zx} = \int_{k_-}^{k_+} dY \int_{m_-}^{m_+} dZ \frac{Z}{(n_-^2 + Y^2 + Z^2)^{3/2}}, \quad (\text{B7})$$

$$T_{n,k,m}^{zy} = \int_{n_-}^{n_+} dX \int_{m_-}^{m_+} dZ \frac{Z}{(X^2 + k_-^2 + Z^2)^{3/2}}, \quad (\text{B8})$$

$$T_{n,k,m}^{zz} = \int_{n_-}^{n_+} dX \int_{k_-}^{k_+} dY \frac{m_-}{(X^2 + Y^2 + m_-^2)^{3/2}}. \quad (\text{B9})$$

After integration one obtains

$$T_{n,k,m}^{xx} = \gamma(m_+, k_+, n_-) - \gamma(m_-, k_+, n_-) - \gamma(m_+, k_-, n_-) + \gamma(m_-, k_-, n_-), \quad (\text{B10})$$

where we introduced the function

$$\gamma(n, k, m) = \arctan\left(\frac{nk}{m\sqrt{n^2 + k^2 + m^2}}\right), \quad (\text{B11})$$

and

$$T_{n,k,m}^{xy} = \ln\left[\frac{(m_+ + \sqrt{n_-^2 + k_-^2 + m_+^2})}{(m_+ + \sqrt{n_+^2 + k_-^2 + m_+^2})}\right] + \ln\left[\frac{(m_- + \sqrt{n_+^2 + k_-^2 + m_-^2})}{(m_- + \sqrt{n_-^2 + k_-^2 + m_-^2})}\right]. \quad (\text{B12})$$

For symmetry reasons the other components of the tensor \hat{T} can be expressed as

$$T_{n,k,m}^{yy} = T_{k,n,m}^{xx}, \quad T_{n,k,m}^{zz} = T_{m,k,n}^{xx}, \quad (\text{B13})$$

$$T_{n,k,m}^{xz} = T_{n,m,k}^{xy}, \quad T_{n,k,m}^{yx} = T_{k,n,m}^{xy}, \quad (\text{B14})$$

$$T_{n,k,m}^{yz} = T_{k,m,n}^{xy}, \quad T_{n,k,m}^{zx} = T_{m,n,k}^{xy}, \quad (\text{B15})$$

$$T_{n,k,m}^{zy} = T_{m,k,n}^{xy}. \quad (\text{B16})$$

For calculation of the field-component variances using Eq. (11) the correlation functions of the charge densities have to

be obtained first. They appear to be diagonal in Cartesian indices β, β' and involve only next-neighbor indices n, k, m

$$\langle \sigma_{n,k,m}^x \sigma_{n',k',m'}^x \rangle = P_s^2 a_3 \delta_{k,k'} \delta_{m,m'} (2\delta_{n,n'} - \delta_{n,n'-1} - \delta_{n,n'+1})$$

$$\langle \sigma_{n,k,m}^y \sigma_{n',k',m'}^y \rangle = P_s^2 a_3 \delta_{n,n'} \delta_{m,m'} (2\delta_{k,k'} - \delta_{k,k'-1} - \delta_{k,k'+1})$$

$$\begin{aligned} \langle \sigma_{n,k,m}^z \sigma_{n',k',m'}^z \rangle &= P_s^2 (a_1 - a_2) \delta_{n,n'} \delta_{k,k'} \\ &\quad \times (2\delta_{m,m'} - \delta_{m,m'-1} - \delta_{m,m'+1}) \end{aligned} \quad (\text{B17})$$

with constants

$$a_1 = \langle \cos(\theta_{n,k,m})^2 \rangle = \frac{1}{3} + \frac{2}{\pi\sqrt{3}} = 0.701,$$

$$a_2 = \langle \cos(\theta_{n,k,m})^2 \rangle = \frac{18}{\pi^2} \arcsin^2(\sqrt{1/3}) = 0.691,$$

$$a_3 = \langle \sin(\theta_{n,k,m})^2 \sin(\varphi_{n,k,m})^2 \rangle = \frac{\pi - \sqrt{3}}{3\pi} = 0.15. \quad (\text{B18})$$

This is followed by expressions for the field-component variances

$$\begin{aligned} \langle (\Delta E_d^\alpha)^2 \rangle &= \left(\frac{P_s}{4\pi\epsilon_0\epsilon_f}\right)^2 \sum_{n,k,m} [a_3 T_{n,k,m}^{\alpha x} (2T_{n,k,m}^{\alpha x} - T_{n-1,k,m}^{\alpha x} \\ &\quad - T_{n+1,k,m}^{\alpha x}) + a_3 T_{n,k,m}^{\alpha y} (2T_{n,k,m}^{\alpha y} - T_{n,k-1,m}^{\alpha y} - T_{n,k+1,m}^{\alpha y}) \\ &\quad + (a_1 - a_2) T_{n,k,m}^{\alpha z} (2T_{n,k,m}^{\alpha z} - T_{n,k,m-1}^{\alpha z} - T_{n,k,m+1}^{\alpha z})] \end{aligned} \quad (\text{B19})$$

containing well converging series. The sums in the last formula are evaluated numerically resulting in formula (12).

The sum of correlation functions between the polarization and field arising in the Gibbs energy, Eq. (15), is position independent and can be evaluated, for example, for the central grain with $n=k=m=0$ using Eq. (10)

$$\begin{aligned} \Delta G_+(0) &= -\frac{P_s^2 \Omega}{8\pi\epsilon_0\epsilon_f} [a_3 (T_{1,0,0}^{xx} - T_{0,0,0}^{xx}) + a_3 (T_{0,1,0}^{yy} - T_{0,0,0}^{yy}) \\ &\quad + (a_1 - a_2) (T_{0,0,1}^{zz} - T_{0,0,0}^{zz})] \end{aligned} \quad (\text{B20})$$

resulting in Eq. (15).

APPENDIX C: THERMODYNAMIC RELATIONS FOR A FERROELECTRIC SAMPLE IN AN EXTERNAL ELECTRIC FIELD

An expression for the Gibbs free energy of a ferroelectric body subject to an external electric field is given by³⁵

$$\begin{aligned} G &= \int dV \left(F_0 - \frac{1}{2} \epsilon_0 \mathbf{E}(\hat{\epsilon}, \mathbf{E}) - \mathbf{E} \mathbf{P}_s \right) \\ &= \int dV \left(F_0 - \frac{1}{2} \mathbf{E} \mathbf{D} - \frac{1}{2} \mathbf{E} \mathbf{P}_s \right), \end{aligned} \quad (\text{C1})$$

where \mathbf{E} and $\mathbf{D} = \mathbf{P}_s + \epsilon_0 \hat{\epsilon} \mathbf{E}$ are the total electrical field and

the electrical displacement, respectively, \mathbf{P}_s denotes the local spontaneous polarization, and $\hat{\epsilon}$, the relative permittivity tensor. The energy F_0 depends on temperature and the material density only, while piezoelectric contributions are not considered. The integration in this expression is over the whole space excluding the volume of the conductors creating the external field.

Using the potential presentation of the electric field $\mathbf{E}=-\nabla\phi$ and the fact that $\nabla\mathbf{D}=0$ due to the absence of the external charges in the ferroelectric body one can transform $\mathbf{E}\mathbf{D}=-\nabla(\phi\mathbf{D})$ and then convert the integration of the respective term in Eq. (C1) to the integral over the surfaces of the conductors creating the external field. Since these surfaces are at constant potentials ϕ_k and the surface charge densities

are given by the normal component of the electric displacement, D_n , the Gibbs free energy can be transformed to

$$G = \mathcal{F}_0 - \frac{1}{2} \sum_k Q_k \phi_k - \frac{1}{2} \int dV \mathbf{E} \mathbf{P}_s, \quad (\text{C2})$$

where Q_k are the total charges at the conductors numerated by the index k and \mathcal{F}_0 depends only on temperature and the material density. In contrast to Eq. (C1) the integration in the last equation is over the volume of the dielectric body only since outside of the body the polarization vanishes. In equilibrium, the Gibbs free energy is minimum with respect to parameters involved³⁵ when the potentials ϕ_k at the conductors are kept constant.

*yugen@tgm.tu-darmstadt.de

- ¹K. W. Plessner, Proc. Phys. Soc. London, Sect. B **69**, 1261 (1956).
- ²K. Okazaki, Memoirs of the Defense Academy of Japan **5**, 99 (1965).
- ³K. Okazaki, Memoirs of the Defense Academy of Japan **5**, 341 (1966).
- ⁴K. Okazaki, *Ceramics Engineering for Dielectrics* (Gakken Shya, Tokyo, 1969).
- ⁵M. Takahashi, Jpn. J. Appl. Phys., Part 1 **9**, 1236 (1970).
- ⁶H. Thomann, Ferroelectrics **4**, 141 (1972).
- ⁷G. Arlt and H. Neumann, Ferroelectrics **87**, 109 (1988).
- ⁸R. Lohkämper, H. Neumann, and G. Arlt, J. Appl. Phys. **68**, 4220 (1990).
- ⁹W. L. Warren, K. Vanheusden, D. Dimos, G. E. Pike, and B. A. Tuttle, J. Am. Ceram. Soc. **79**, 536 (1996).
- ¹⁰L. X. Zhang and X. Ren, Phys. Rev. B **73**, 094121 (2006).
- ¹¹Rudiger-A. Eichel, P. Erhart, P. Träskelin, K. Albe, H. Kungl, and M. J. Hoffmann, Phys. Rev. Lett. **100**, 095504 (2008).
- ¹²L. X. Zhang, E. Erdem, X. Ren, and R.-A. Eichel, Appl. Phys. Lett. **93**, 202901 (2008).
- ¹³K. Carl and K. H. Härdtl, Ferroelectrics **17**, 473 (1978).
- ¹⁴S. Takahashi, Ferroelectrics **41**, 143 (1982).
- ¹⁵T. B. Weston, A. H. Webster, and V. M. McNamara, J. Am. Ceram. Soc. **52**, 253 (1969).
- ¹⁶H.-J. Kleebe, S. Lauterbach, L. Silvestroni, H. Kungl, M. Hoffmann, E. Erdem, and R.-A. Eichel, Appl. Phys. Lett. **94**, 142901 (2009).
- ¹⁷D. C. Lupascu, Y. A. Genenko, and N. Balke, J. Am. Ceram. Soc. **89**, 224 (2006).

- ¹⁸Y. A. Genenko and D. C. Lupascu, Phys. Rev. B **75**, 184107 (2007); **76**, 149907(E) (2007).
- ¹⁹Y. A. Genenko, Phys. Rev. B **78**, 214103 (2008).
- ²⁰N. Balke, T. Granzow, and J. Rödel, J. Appl. Phys. **105**, 104105 (2009).
- ²¹H. G. Baerwald, Phys. Rev. **105**, 480 (1957).
- ²²N. Uchida and T. Ikeda, Jpn. J. Appl. Phys., Part 1 **6**, 1079 (1967).
- ²³D. M. Smyth, Ferroelectrics **151**, 115 (1994).
- ²⁴C. J. Brennan, Integr. Ferroelectr. **7**, 93 (1995).
- ²⁵M. V. Raymond and D. M. Smyth, J. Phys. Chem. Solids **57**, 1507 (1996).
- ²⁶D. M. Smyth, J. Electroceram. **11**, 89 (2003).
- ²⁷R. M. Waser, J. Am. Ceram. Soc. **74**, 1934 (1991).
- ²⁸A. Molak, M. Paluch, and S. Pawlus, Phys. Rev. B **78**, 134207 (2008).
- ²⁹A. Molak and K. Szot, Phys. Status Solidi (RRL) **3**, 127 (2009).
- ³⁰P. M. Jones, D. E. Gallardo, and S. Dunn, Chem. Mater. **20**, 5901 (2008).
- ³¹S. Gottschalk, S. Flege, and A. Balogh, J. Appl. Phys. **104**, 114106 (2008).
- ³²M. Hammer and M. J. Hoffmann, J. Am. Ceram. Soc. **81**, 3277 (1998).
- ³³M. Morozov, Ph.D. thesis, École Polytechnique Fédérale de Lausanne, 2005.
- ³⁴M. U. Farooq, R. Villaurrutia, I. Maclaren, H. Kungl, M. J. Hoffmann, J. J. Fundenberger, and E. Bouzy, J. Microsc. **230**, 445 (2008).
- ³⁵L. D. Landau and E. M. Lifshitz, *Electrodynamics of Continuous Media* (Pergamon, Oxford, 1963).